PERGAMON

International Journal of Solids and Structures 37 (2000) 6107–6130

INTERNATIONAL JOURNAL OF SOLIDS and STRUCTURES

www.elsevier.com/locate/ijsolstr

Transient elastodynamic antiplane crack analysis of anisotropic solids

Ch. Zhang

Department of Civil Engineering, Hochschule Zittau/Görlitz (FH), University of Applied Sciences, 02763 Zittau, Germany

Received 1 April 1999

Abstract

Transient elastodynamic analysis of an antiplane crack in anisotropic solids is presented. A time-domain traction boundary integral equation (BIE) method is applied for this purpose. The traction BIE is hypersingular and has the crack-opening-displacement as its fundamental unknown quantity. Unlike the usual time-domain BIE method the present formulation applies a convolution quadrature developed by Lubich (Lubich, C., 1988a,b. Convolution quadrature and discretized operational calculus. Numer. Math. 52, 129–145 (Part I), 413–425 (Part II)) which requires only the Laplace-domain instead of the time-domain Green's functions. The spatial variation of the crack-opening-displacement is approximated by an infinite series of Chebyshev polynomials which take the local behavior of the crack-opening-displacement at crack-tips into account. By using a Galerkin method, the time-domain BIE is converted into a system of linear algebraic equations which can be solved step by step. Special attention is devoted to the computation of dynamic stress intensity factors of an antiplane crack in generally anisotropic solids. Numerical results for isotropic solids are presented and compared with the well-known analytical results of Thau and Lu (Thau, S.A., Lu, T.H., 1970. Diffraction of transient horizontal shear waves by a finite crack and a finite rigid ribbon. Int. J. Enggn. Sci. 8, 857–874), to check the accuracy and efficiency of the present time-domain BIE method. The effect of the material anisotropy on the dynamic stress intensity factors is analyzed via several numerical examples.

Keywords: Anisotropic solids; Elastodynamics; Transient dynamic crack analysis; Elastic wave scattering; Boundary integral equations

1. Introduction

Elastodynamic crack analysis of anisotropic solids is of particular interest to ultrasonic quantitative non-destructive evaluation and to linear elastic fracture mechanics. Since the location, orientation, shape

E-mail address: c.zhang@htw-zittau.de (C. Zhang).

0020-7683/00/$ - see front matter
PII: S0020-7683(99)00260-7

and size of pre-existing interior or surface cracks are directly related to scattered elastic waves, useful information can be extracted from ultrasonic nondestructive measurements for detecting and quantitatively characterizing crack-like defects in anisotropic materials. Once crack-like defects have been detected and characterized, the concepts of linear elastic fracture mechanics can be applied to assess the initiation and growth of pre-existing cracks under static or dynamic loading conditions. Material anisotropy may occur in many solids such as composites, piezoelectric ceramics, ice and diamond. Crack-like defects in such solids may be induced due to manufacturing or inservice conditions.

Several investigations on elastodynamic crack analysis of anisotropic solids can be found in literature. Elastodynamic stress intensity factors due to incident plane time-harmonic elastic waves have been presented by Ohyoshi (1973a), Zhang and Gross (1993) for antiplane cracks, and by Ohyoshi (1973b) and Dhawan (1982, 1983) for inplane cracks in transversely isotropic solids. Diffraction of plane time-harmonic elastic waves has been investigated by Lobanov and Novichkov (1981) for an antiplane crack in an orthotropic half-space, and by Norris and Achenbach (1984) for a semi-infinite inplane crack in an infinite transversely isotropic material. Dynamic response analysis has been performed by Karim and Kundu (1988) for layered anisotropic half-spaces with antiplane interface cracks and by Karim and Kundu (1991) for an orthotropic half-space with a subsurface in-plane crack. Scattering and diffraction of SH-waves by multiple planar cracks in an anisotropic half-space has been analyzed by Ang et al. (1993) via a hypersingular integral equation formulation. Transient elastodynamic stress intensity factors due to impact loading have been given by Kassir and Bandyopadhyay (1983), Shindo et al. (1986), and Ang (1987) for an inplane crack in an infinite transversely isotropic solid, by Shindo and Nozaki (1987) for a transversely isotropic cylinder with a penny-shaped crack, by Ang (1988) for an inplane crack in a transversely isotropic layered material, and by Kuo (1984a, 1984b) for an interface crack between orthotropic and fully anisotropic half-spaces. The interaction of time-harmonic elastic waves with a penny-shaped crack in transversely isotropic materials has been analyzed by Tsai (1973, 1982, 1988, 1989) who calculated the elastodynamic stress intensity factors, by Kundu (1990), and by Kundu and Boström (1991, 1992) who computed the crack-opening-displacements and the scattered far-field. A steadily moving inplane crack in an orthotropic material has been studied by Kassir and Tse (1983) and Piva (1986, 1987), while closed form solutions for an antiplane crack moving in an orthotropic layer of finite thickness have been given by Danyluk and Singh (1984). A periodic array of collinear antiplane cracks in transversely isotropic solids has been analyzed by Zhang (1992). Recent investigations on the subject include the wave scattering analysis of Liu and Achenbach (1995) for anisotropic laminated plates with cracks via the strip element method, the time-harmonic analysis by Sarkar et al. (1995) for three coplanar cracks, Itou (1996) for two collinear cracks, and Itou and Haliding (1997) for two parallel cracks in an orthotropic medium, the transient analysis by Rizza and Nair (1998) for a penny-shaped crack in a transversely isotropic material under non-axisymmetric impact loads, the dynamic response treatment of Rubio-Gonzalez and Mason (1999) for finite cracks in orthotropic materials due to concentrated impact shear loads, the wave scattering analysis by Shen and Kuang (1998) for an interface crack in laminated anisotropic media, the transient response analysis of Pramanik et al. (1998) for an interface crack between two anisotropic solids under a pair of antiplane point impact loading on the crack-faces, the intersonic shear crack propagation investigation by Piva and Hasan (1996) for orthotropic materials, the stress intensity factors computations by Das and Patra (1998) for moving interfacial crack between bonded dissimilar fixed orthotropic layers, and the crack propagation modelling in anisotropic media by Padovan (1998). Boundary element method has been presented by Domínguez and Sáez (1998), Sáez and Domínguez (1999) for time-harmonic wave scattering analysis in transversely isotropic solids with penny-shaped cracks, and by Albuquerque et al. (1999) for two-dimensional cracked anisotropic media. Most of the previous studies on elastodynamic crack analysis of anisotropic solids have been limited to transversely isotropic or orthotropic solids. This case arises for instance in unidirectionally fiber-reinforced composites and cross-plied laminates when the crack plane

coincides with one of the principal axes of material symmetry. If the crack plane, however, is aligned with respect to the axes of material symmetry, the assumption of a transverse isotropy is no longer valid and a general anisotropy arises. Ultrasonic crack detection in solids of general anisotropy has been investigated by Mattsson (1996), Niklasson (1997), Mattsson and Niklasson (1997), and Mattsson et al. (1997).

In this paper, transient elastodynamic crack analysis is performed for an infinite solid of general anisotropy and for a state of antiplane strain. A time-domain traction boundary integral equation (BIE) method is applied for this purpose. In Section 2, the initial-boundary value problem of transient wave scattering by a finite crack of general shape is formulated as a traction BIE in time-domain. This traction BIE is hypersingular and has the crack-opening-displacement as its fundamental unknown quantity. A time-stepping scheme for solving the hypersingular time-domain BIE is presented in Section 3. To simplify the analysis, a straight crack is assumed. Unlike the usual time-stepping scheme frequently applied in solving time-domain BIEs, the present method uses a convolution quadrature developed by Lubich (1988a, 1988b). The convolution quadrature of Lubich (1988a, 1988b) bases on a multistep method and it uses the Laplace-domain instead of the time-domain Green's functions. The spatial variation of the crack-opening displacement (COD) is approximated by a series of Chebyshev polynomials which take the proper local behavior of the crack-opening-displacement at crack-tips into account. By adopting a Galerkin method, a system of linear algebraic equations for the expansion coefficients is obtained, which can be solved step by step. The problem in the Laplace-domain is discussed in Section 4, to derive the Green's functions and to evaluate the system matrix in the Laplace-domain, which are needed in the present time-stepping scheme. Once the crack-opening-displacement has been determined via the time-stepping scheme, the elastodynamic stress intensity factors, the displacement and the stress fields at an arbitrary point can be computed in a simple manner. The required fundamental equations for doing this are given in Sections 5 and 6. Numerical results and discussions are presented in Section 7. To test the accuracy and efficiency of the present time-domain BIE method, numerical results for isotropic solids are given and compared with the well-known analytical results of Thau and Lu (1970). It shows that the present method is highly accurate and stable. Several numerical examples for elastic solids of general anisotropy are shown to analyze the effects of the material anisotropy on the time-dependent elastodynamic stress intensity factors.

2. Problem statement and time-domain BIE

We consider an infinite, homogeneous, anisotropic, and linearly elastic solid containing a finite crack of an arbitrary shape as shown in Fig. 1. The solid is subjected to an incident transient plane SH-wave, and the deformation of the solid is thus in a state of antiplane strain. The non-zero quantities are the displacement component u_3 in the x_3-direction, and the shear stress components $\sigma_{3\alpha}$ ($\alpha = 1, 2$). The cracked anisotropic solid is described by the equation of motion

$$\sigma_{3\alpha,\,\alpha} = \rho \ddot{u}_3, \tag{1}$$

the Hooke's law

$$\begin{Bmatrix} \sigma_{31} \\ \sigma_{32} \end{Bmatrix} = \begin{bmatrix} C_{55} & C_{45} \\ C_{45} & C_{44} \end{bmatrix} \begin{Bmatrix} u_{3,\,1} \\ u_{3,\,2} \end{Bmatrix}, \tag{2}$$

the initial conditions

$$u_3(\mathbf{x}, t) = \dot{u}_3(\mathbf{x}, t) = 0, \quad \text{for } t = 0, \tag{3}$$

and the traction-free boundary condition on the crack-faces

$$f_3(\mathbf{x}, t) = \sigma_{3\alpha}(\mathbf{x}, t)n_\alpha(\mathbf{x}) = 0, \quad \mathbf{x} \in \Gamma_c. \tag{4}$$

Here, ρ is the mass density, C_{44}, C_{45} and C_{55} are the elastic constants, $\Gamma_c = \Gamma_c^+ + \Gamma_c^-$ are the crack-faces, and n_α is the unit normal vector. Also, a comma after a quantity represents the partial derivative with respect to spatial variables, and superscript dots stand for the temporal derivatives of the quantity. The conventional summation rule over double indices is implied.

By substituting Eq. (2) into Eq. (1) the equation of motion in terms of the displacement component u_3 can be written as

$$C_{55}u_{3,\,11} + 2C_{45}u_{3,\,12} + C_{44}u_{3,\,22} = \rho\ddot{u}_3. \tag{5}$$

The interaction of an incident wave with the crack induces scattered waves. The total wave field can be written as a sum of the incident wave field and the scattered wave field

$$u_3 = u_3^{\text{in}} + u_3^{\text{sc}}, \qquad \sigma_{3\alpha} = \sigma_{3\alpha}^{\text{in}} + \sigma_{3\alpha}^{\text{sc}}, \tag{6}$$

where u_3^{in} and $\sigma_{3\alpha}^{\text{in}}$ represent the displacement and the stress components of the incident wave field in the absence of the crack, while u_3^{sc} and $\sigma_{3\alpha}^{\text{sc}}$ denote the corresponding displacement and stress components of the scattered wave field due to the interaction of the incident wave with the crack. The incident wave field is assumed to be known, while the scattered wave field is unknown and has to be determined. The scattered wave field should satisfy the equation of motion (1) or (5), Hooke's law (2), the initial conditions (3), and the boundary condition (4) which can be rewritten as

$$f_3^{\text{sc}}(\mathbf{x}, t) = -f_3^{\text{in}}(\mathbf{x}, t), \quad \mathbf{x} \in \Gamma_c. \tag{7}$$

The scattered displacement $u_3^{\text{sc}}(\mathbf{x}, t)$ can be represented by a boundary integral of the form

$$u_3^{\text{sc}}(\mathbf{x}, t) = \int_{\Gamma_c^+} \sigma_{3\alpha 3}^{\text{G}}(\mathbf{x}, \mathbf{y}; t, \tau) * \Delta u_3(\mathbf{y}, \tau)n_\alpha(\mathbf{y})\, \mathrm{d}s, \quad \mathbf{x} \notin \Gamma_c^+, \tag{8}$$

where $\sigma_{3\alpha 3}^{\text{G}}(\mathbf{x}, \mathbf{y}; t, \tau)$ is the stress Green's function, $\Delta u_3(\mathbf{y}, \tau)$ is the crack-opening-displacement

$$\Delta u_3(\mathbf{y}, \tau) = u_3\big(\mathbf{y} \in \Gamma_c^+, \tau\big) - u_3\big(\mathbf{y} \in \Gamma_c^-, \tau\big), \tag{9}$$

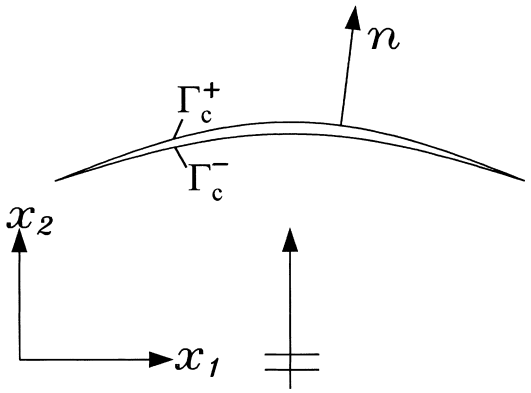

Fig. 1. A crack of arbitrary shape.

and an asterisk $*$ denotes Riemann convolution defined by

$$g(\mathbf{x}, t) * h(\mathbf{x}, t) = \int_0^t g(\mathbf{x}, t-\tau) h(\mathbf{x}, \tau)\, \mathrm{d}\tau. \tag{10}$$

Substitution of Eq. (8) into Hooke's law (2) results in an integral representation formula for the traction component $f_3^{\mathrm{sc}}(\mathbf{x}, t)$

$$f_3^{\mathrm{sc}}(\mathbf{x}, t) = n_\alpha(\mathbf{x}) \int_{\Gamma_c^+} T_{3\alpha 3}^{\mathrm{G}}(\mathbf{x}, \mathbf{y}; t, \tau) * \Delta u_3(\mathbf{y}, \tau)\, \mathrm{d}s, \quad \mathbf{x} \notin \Gamma_c^+, \tag{11}$$

where

$$\begin{Bmatrix} T_{313}^{\mathrm{G}} \\ T_{323}^{\mathrm{G}} \end{Bmatrix} = \begin{bmatrix} C_{55} & C_{45} \\ C_{45} & C_{44} \end{bmatrix} \begin{Bmatrix} \dfrac{\partial \sigma_{3\beta 3}^{\mathrm{G}}}{\partial x_1} n_\beta \\ \dfrac{\partial \sigma_{3\beta 3}^{\mathrm{G}}}{\partial x_2} n_\beta \end{Bmatrix}. \tag{12}$$

By taking the limit process $\mathbf{x} \to \Gamma_c^+$ and considering the traction-free boundary condition (4) or (7), a time-domain traction BIE is obtained as

$$n_\alpha(\mathbf{x}) \int_{\Gamma_c^+} T_{3\alpha 3}^{\mathrm{G}}(\mathbf{x}, \mathbf{y}; t, \tau) * \Delta u_3(\mathbf{y}, \tau)\, \mathrm{d}s = -f_3^{\mathrm{in}}(\mathbf{x}, t), \quad \mathbf{x} \in \Gamma_c^+, \tag{13}$$

in which the crack-opening-displacement Δu_3 is the fundamental unknown quantity of the traction BIE. Note here that the time-domain traction BIE (13) is hypersingular since $T_{3\alpha 3}^{\mathrm{G}}(\mathbf{x}, \mathbf{y}; t, \tau)$ behaves as (see Wang and Achenbach, 1994; Wang et al., 1996)

$$T_{3\alpha 3}^{\mathrm{G}}(\mathbf{x}, \mathbf{y}; t, \tau) \propto \frac{1}{|\mathbf{x} - \mathbf{y}|^2}, \quad \text{for } \mathbf{x} \to \mathbf{y}. \tag{14}$$

The hypersingular integral in Eq. (13) has to be understood in the sense of Hadamard finite-part integral. In general, the hypersingular BIE (13) can be solved by three different methods, namely the Galerkin method, the regularization method and the direct method. In this paper, a Galerkin method will be used. Note here that an explicit expression for the time-domain Green's function $T_{3\alpha 3}^{\mathrm{G}}(\mathbf{x}, \mathbf{y}; t, \tau)$ itself is not required in the present method as will be seen in the following sections. In lieu of this, its Laplace transform $\hat{T}_{3\alpha 3}^{\mathrm{G}}(\mathbf{x}, \mathbf{y}; p)$ plays a more important role and should have a simple mathematical structure.

3. A time-stepping scheme

In this section, a time-stepping scheme is presented for solving the hypersingular time-domain BIE (13). The scheme uses the convolution quadrature of Lubich (1988a, 1988b) for evaluating the temporal convolution and a Galerkin method for the spatial approximation of the unknown crack-opening-displacement. The essential features of the convolution quadrature of Lubich (1988a, 1988b) are summarized in Appendix A. To simplify the analysis, a straight crack of length $2a$ as shown in Fig. 2 will be assumed in what follows. In this case, the hypersingular BIE (13) takes the following form

$$\int_{-a}^{+a} T^{\mathrm{G}}_{3\alpha 3}(x_1, y_1; t, \tau) * \Delta u_3(y_1, \tau)\, \mathrm{d}y_1 = -\sigma^{\mathrm{in}}_{32}(x_1, t), \quad x_1 \in [-a, +a], \tag{15}$$

The unknown crack opening displacement $\Delta u_3(y_1, \tau)$ is expanded into an infinite series of the form

$$\Delta u_3(y_1, \tau) = \sqrt{a^2 - y_1^2} \sum_{k=1}^{\infty} c_k(\tau) U_{k-1}(y_1/a), \tag{16}$$

where $c_k(\tau)$ are the unknown time-dependent expansion coefficients and $U_{k-1}(y_1/a)$ are the Chebyshev polynomials of second kind. Substituting Eq. (16) into Eq. (15), multiplying both sides by $\sqrt{a^2 - x_1^2} U_{l-1}(x_1/a)$ and integrating with respect to x_1 from $-a$ to $+a$, the following equation is obtained

$$\sum_{k=1}^{\infty} \int_{-a}^{+a} \sqrt{a^2 - x_1^2} U_{l-1}(x_1/a) \int_{-a}^{+a} \sqrt{a^2 - y_1^2} U_{k-1}(y_1/a) T^{\mathrm{G}}_{323}(x_1, y_1; t, \tau) * c_k(\tau)\, \mathrm{d}y_1\, \mathrm{d}x_1$$

$$= -\int_{-a}^{+a} \sigma^{\mathrm{in}}_{32}(x_1, t) \sqrt{a^2 - x_1^2} U_{l-1}(x_1/a)\, \mathrm{d}x_1, \quad l = 1, 2, \ldots, \infty. \tag{17}$$

The application of the convolution quadrature formula (see Appendix A)

$$f(t) = g(t) * h(t) = \int_0^t g(t - \tau) h(\tau)\, \mathrm{d}\tau \quad \Longrightarrow \quad f(n\Delta t) = \sum_{j=0}^{n} \omega_{n-j}(\Delta t) h(j\Delta t) \tag{18}$$

to Eq. (17) leads to a system of linear algebraic equations for the expansion coefficients

$$\sum_{j=0}^{n-1} \mathbf{A}^{n-j} \mathbf{c}^{\,j} = \mathbf{f}^n, \quad n = 1, 2, \ldots, N, \tag{19}$$

where the time variable t is devided into N equal time-steps Δt and

$$\mathbf{A}^{n-j} = \left(A^{n-j}_{kl}\right); \quad \mathbf{c}^{\,j} = \left(c_l^{\,j}\right); \quad \mathbf{f}^n = \left(f^{\,n}_{l}\right), \tag{20}$$

with upper indices indicating the time-steps. The system matrix in Eq. (19) corresponds to the

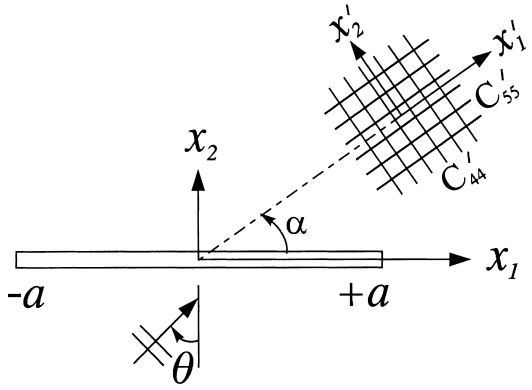

Fig. 2. A straight crack of length $2a$.

integration weights $\omega_{n-j}(\Delta t)$ in the convolution quadrature (18). The system matrix and the right-hand side of Eq. (19) are given by

$$\mathbf{A}^n = \frac{r^{-n}}{M}\sum_{m=0}^{M-1}\hat{\mathbf{A}}(p_m)\mathrm{e}^{-2\pi i\cdot nm/M}, \tag{21}$$

$$f_l^n = (-1)^{l+1}\int_{-a}^{+a}\sigma_{32}^{\mathrm{in}}(x_1, n\Delta t)\sqrt{a^2 - x_1^2}\,U_{l-1}(x_1/a)\,\mathrm{d}x_1. \tag{22}$$

In Eq. (21)

$$p_m = \delta(\zeta_m)/\Delta t; \quad \delta(\zeta_m) = \sum_{j=1}^{2}(1-\zeta_m)^j/j; \quad \zeta_m = r\mathrm{e}^{2\pi i\cdot m/M}. \tag{23}$$

By choosing $M = N$ and $r^N = \sqrt{\epsilon}$ it can be shown (Lubich, 1988a, 1988b) that the error in $\mathbf{A}^n$ in the present convolution quadrature method is of the order $O(\sqrt{\epsilon})$, where ϵ is the numerical error arised by computing the Laplace transform $\hat{\mathbf{A}}(p_m)$ of the system matrix. The system matrix in the Laplace-domain has the following form

$$\hat{A}_{kl}(p) = (-1)^l\int_{-a}^{+a}\sqrt{a^2 - x_1^2}\,U_{l-1}(x_1/a)\int_{-a}^{+a}\sqrt{a^2 - y_1^2}\,U_{k-1}(y_1/a)\hat{T}_{323}^{\mathrm{G}}(x_1, y_1; p)\,\mathrm{d}y_1\,\mathrm{d}x_1, \tag{24}$$

where $\hat{T}_{323}^{\mathrm{G}}(x_1, y_1; p)$ is the Green's function in the Laplace-domain. An essential feature of the present time-domain method is that it uses the Laplace-domain instead of the time-domain Green's functions which are frequently applied in the usual time-domain BIE formulation. The system matrix defined by Eq. (21) is symmetric, real-valued and it is just the real-part of the right-hand side of Eq. (21). The evaluation of Eq. (21) can be performed very efficiently by using the Fast Fourier Transform (FFT). The Green's functions and the computation of the system matrix $\hat{\mathbf{A}}(p)$ in the Laplace transform domain are presented in the next section.

By considering the zero initial conditions (3) the following time-stepping scheme is obtained from Eq. (19)

$$\mathbf{c}^n = (\mathbf{A}^0)^{-1}\left(\mathbf{f}^n - \sum_{j=1}^{n-1}\mathbf{A}^{n-j}\mathbf{c}^j\right), \quad n = 1, 2, \ldots, N, \tag{25}$$

where $(\mathbf{A}^0)^{-1}$ is the inverse matrix of $\mathbf{A}^0$ at the time-step $n = 0$. The unknown time-dependent expansion coefficient $\boldsymbol{c}^n$ can be obtained by solving equations (25) step by step.

In passing, some comments on the present time-domain BIE method should be made. The usual time-domain BIE method applies time-domain Green's functions and the arising temporal convolution integrals with respect to the time variable can be evaluated analytically, when the time-domain Green's functions have a simple mathematical structure and a polynomial temporal shape function (constant, linear or higher order) for the unknown boundary data is used. The main difficulty of this kind of time-domain BIE formulation is the proper choice of the time-step. A too small time-step gives rise to unstable numerical solution, while a too large time-step leads to a numerical damping of the solution. The present time-domain BIE formulation uses, on the other hand, a convolution quadrature based on a multistep method, and it requires only the Laplace-domain Green's functions. A comparative study of this method to the usual time-domain and Laplace-domain BIE formulations has been performed by

Gaul and Schanz (1999) for viscoelastic solids. Other recent research works based on the convolution quadrature method of Lubich (1988a, 1988b) have been carried out by Schanz and Antes (1997a, 1997b) and Schanz (1998, 1999) for visco- and elastodynamic initial-boundary value problems in solid mechanics. These authors have used the collocation method for the spatial discretization of the BIEs and they have shown that the time-domain BIE method based on the convolution quadrature of Lubich (1988a, 1988b) is more stable and less sensitive to the choice of the time-step than in the usual time-domain BIE method. Since this method is less sensitive to the choice of the time-step, it is also advantageous over the Laplace-domain BIE method, where the accuracy of the inverse transform may depend strongly on the proper choice of the real part of the transform parameter. Another advantage of the method is that it can also be applied to cases where only the Laplace-domain Green's functions are available in simple forms, while the corresponding time-domain Green's functions are either not available or they do not have a simple mathematical structure. Well-known examples are the dynamic viscoelastic and the dynamic poreelastic Green's functions.

4. Evaluation of the system matrix in Laplace-domain

To compute the time-dependent system matrix $\mathbf{A}^n$ by Eq. (21), its Laplace transform $\hat{\mathbf{A}}(p)$ is required. In this section, the generic problem in the Laplace transform domain is described, the Green's function $\hat{T}^{\mathrm{G}}_{323}(x_1, y_1; p)$ and the system matrix $\hat{\mathbf{A}}(p)$ are derived.

By applying the one-sided Laplace transform defined by

$$\hat{f}(p) = \int_0^\infty f(t)\mathrm{e}^{-pt}\,\mathrm{d}t; \quad f(t) = \frac{1}{2\pi i}\int_{C-i\infty}^{C+i\infty} \hat{f}(p)\mathrm{e}^{pt}\,\mathrm{d}p; \tag{26}$$

to Eq. (5) the equation of motion can be written as

$$C_{55}\hat{u}_{3,11} + 2C_{45}\hat{u}_{3,12} + C_{44}\hat{u}_{3,22} = \rho p^2 \hat{u}_3, \tag{27}$$

where C in Eq. (26) is a real constant and p is a transform parameter. The boundary and the continuity conditions on the crack-faces $|x_1| \le a$ and the crack-plane $|x_1| \le \infty$ can be stated as

$$\hat{\sigma}^{\mathrm{sc}}_{32}(x_1, 0) = -\hat{\sigma}^{\mathrm{in}}_{32}(x_1, 0), \quad |x_1| \le a. \tag{28}$$

$$\hat{\sigma}^{\mathrm{sc}}_{32}\left(x_1, 0^+\right) = -\hat{\sigma}^{\mathrm{sc}}_{32}(x_1, 0^-), \quad |x_1| < \infty, \tag{29}$$

$$\hat{u}^{\mathrm{sc}}_{3}\left(x_1, 0^+\right) = \hat{u}^{\mathrm{sc}}_{3}(x_1, 0^-), \quad |x_1| > a. \tag{30}$$

Across the crack-faces, the scattered displacement jumps, i.e.,

$$\hat{u}^{\mathrm{sc}}_{3}\left(x_1, 0^+\right) - \hat{u}^{\mathrm{sc}}_{3}(x_1, 0^-) = \Delta\hat{u}_3(x_1), \quad |x_1| < a, \tag{31}$$

where $\Delta\hat{u}_3(x_1)$ is the crack-opening-displacement in the Laplace transform domain.

The scattered displacement $\hat{u}^{\mathrm{sc}}_3$ satisfying Eq. (27) can be expressed as a Fourier integral of the form

$$\hat{u}_3^{sc}(\mathbf{x}) = \begin{cases} \int_{-\infty}^{\infty} f_1(\xi)\exp\left(i\xi x_1 - \gamma_+ x_2\right) \mathrm{d}\xi, & x_2 > 0, \\ \int_{-\infty}^{\infty} f_2(\xi)\exp\left(i\xi x_1 + \gamma_- x_2\right) \mathrm{d}\xi, & x_2 < 0, \end{cases} \tag{32}$$

where

$$\gamma_\pm = \frac{\gamma \pm C_{45} i\xi}{C_{44}}; \quad \gamma = \sqrt{\left(C_{44}C_{55} - C_{45}^{\,2}\right)\xi^2 + C_{44}\rho p^2}. \tag{33}$$

In Eq. (32), $\mathrm{Re}(\gamma_\pm) \geq 0$, and $f_1(\xi)$ and $f_2(\xi)$ are yet unknown functions.

By substituting Eq. (32) into Hooke's law (2) and by using the continuity condition (29), a relation between f_1 and f_2 is obtained as

$$f_2 = -f_1. \tag{34}$$

Eq. (32) together with Eqs. (30), (31) and (34) result in

$$2\int_{-\infty}^{\infty} f_1(\xi)\exp(i\xi x_1)\,\mathrm{d}\xi = \begin{cases} 0, & |x_1| > a, \\ \Delta\hat{u}_3(x_1), & |x_1| < a. \end{cases} \tag{35}$$

The inversion of Eq. (35) yields

$$f_1(\xi) = \frac{1}{4\pi}\int_{-a}^{+a} \Delta\hat{u}_3(y_1)\exp(-i\xi y_1)\,\mathrm{d}y_1. \tag{36}$$

By substituting Eqs. (34) and (36) into Eq. (32) an expression for $\hat{u}_3^{sc}(\mathbf{x})$ is obtained as

$$\hat{u}_3^{sc}(\mathbf{x}) = \int_{-a}^{+a} \hat{\sigma}_{323}^{G}(\mathbf{x}, \mathbf{y}; p)\Delta\hat{u}_3(y_1)\,\mathrm{d}y_1, \tag{37}$$

where the stress Green's function $\hat{\sigma}_{323}^{G}(\mathbf{x}, \mathbf{y}; p)$ is given by

$$\hat{\sigma}_{323}^{G}(\mathbf{x}, \mathbf{y}; p) = \frac{1}{4\pi}\mathrm{sgn}(x_2 - y_2)\int_{-\infty}^{\infty} \exp\left[i\xi(x_1 - y_1) - \gamma_\pm |x_2 - y_2|\right] \mathrm{d}\xi. \tag{38}$$

Substitution of Eq. (37) into Hooke's law (2) yields a representation integral for the traction component $\hat{f}_3^{sc}(\mathbf{x})$

$$\hat{f}_3^{sc}(\mathbf{x}) = \int_{-a}^{+a} \hat{T}_{323}^{G}(x_1, y_1; p)\Delta\hat{u}_3(y_1)\,\mathrm{d}y_1, \tag{39}$$

where the Green's function $\hat{T}_{323}^{G}(\mathbf{x}, \mathbf{y}; p)$ is given by

$$\hat{T}_{323}^{G}(\mathbf{x}, \mathbf{y}; p) = -\frac{1}{4\pi}\int_{-\infty}^{\infty} \gamma\exp\left[i\xi(x_1 - y_1) - \gamma_\pm |x_2 - y_2|\right] \mathrm{d}\xi. \tag{40}$$

Substituting Eq. (40) into Eq. (24) and using the integration formula

$$\int_{-1}^{1} \sqrt{1-\eta^2}\,U_{k-1}(\eta)\exp(i\alpha\eta)\,\mathrm{d}\eta = \frac{k\pi}{\alpha}J_k(\alpha)\exp\left[i(k-1)\pi/2\right], \tag{41}$$

the system matrix $\hat{A}_{kl}(p)$ defined by Eq. (24) can be evaluated as

$$\hat{A}_{kl}(p) = -\frac{\pi}{4}(-1)^l kla^2 \int_{-\infty}^{\infty} \frac{\gamma}{\xi^2} J_k(-\xi a) J_l(\xi a) \exp\left[3i(k+l)\pi/2\right] \mathrm{d}\xi, \tag{42}$$

in which $J_k(\cdot)$ is the Bessel function of first kind and kth order.

By invoking the relation (Abramowitz and Stegun, 1972)

$$J_k(-z) = (-1)^k J_k(z) \quad (k \text{ integer}), \tag{43}$$

Eq. (42) can be rewritten as

$$\hat{A}_{kl}(p) = \begin{cases} 0, & k+l \text{ odd}, \\ -\dfrac{\pi}{2} i^{k+l} kla^2 \displaystyle\int_0^{\infty} \frac{\gamma}{\xi^2} J_k(\xi a) J_l(\xi a)\, \mathrm{d}\xi, & k+l \text{ even}. \end{cases} \tag{44}$$

Exploiting the orthogonality relation of the Bessel function (Abramowitz and Stegun, 1972)

$$\int_0^{\infty} \frac{1}{z} J_k(z) J_l(z)\, \mathrm{d}z = \frac{\delta_{kl}}{k+l}, \tag{45}$$

Eq. (44) can be recast into

$$\hat{A}_{kl}(p) = -\frac{\pi}{2} i^{k+l} kla^2 \left\{ \left(\frac{\gamma}{\xi^2} - \sqrt{C_{44}C_{55} - C_{45}^2}\frac{1}{\xi} \right) J_k(\xi a) J_l(\xi a)\, \mathrm{d}\xi + \sqrt{C_{44}C_{55} - C_{45}^2}\frac{\delta_{kl}}{k+l} \right\}, \quad k+l \text{ even} \tag{46}$$

By using the asymptotic behavior of the Bessel function (Abramowitz and Stegun, 1972)

$$J_k(z) \sim \sqrt{\frac{2}{\pi z}}, \quad |z| \to \infty, |z| \geq |k|, \tag{47}$$

it can be easily shown that for $\xi \to \infty$ the integrand in Eq. (44) behaves as $1/\xi^2$, while the integrand in Eq. (46) behaves as $1/\xi^4$. Thus, the infinite integral of Eq. (46) converges much more fast than the corresponding integral of Eq. (44) does. The fast convergency of the infinite integral in Eq. (46) is very advantageous for the numerical computation of the system matrix $\hat{A}_{kl}(p)$.

The system matrix $\hat{A}_{kl}(p)$ is symmetric, complex-valued and has to be computed at N discrete values p_m ($m = 0, 1, 2, \ldots, N-1$). Then, the system matrix A_{kl}^n ($n = 0, 1, 2, \ldots, N$) at $N + 1$ time-steps can be evaluated by using Eq. (21). Note here that the present method requires only a numerical integration of a single integral, while the usual Galerkin method in general involves a numerical integration of double or triple integrals in anisotropic cases, since the Laplace-domain Green's functions do not have closed form expressions. Here, the double integrals arised in the system matrix are evaluated analytically which makes the numerical scheme especially effective and attractive.

5. Elastodynamic stress intensity factor

The elastodynamic stress intensity factor of an antiplane crack in anisotropic solids is related to the crack-opening-displacement by

$$K_{III}^{\pm}(t) = \frac{\sqrt{2\pi}}{4}\sqrt{C_{44}C_{55} - C_{45}^{2}}\lim_{x_1 \to \pm a}\frac{1}{\sqrt{a \mp x_1}}\Delta u_3(x_1, t), \tag{48}$$

where "$\pm$" designates the stress intensity factor at the crack tips $x_1 = +a$ and $x_1 = -a$.

Substituting Eq. (16) into Eq. (48) and using the identity (Abramowitz and Stegun, 1972)

$$U_{k-1}(\pm 1) = (\pm 1)^{k-1}k \tag{49}$$

a relation between the elastodynamic stress intensity factor and the expansion coefficients $c_k(t)$ is obtained as

$$K_{III}^{\pm}(t) = \frac{\sqrt{2\pi}}{4}\sqrt{C_{44}C_{55} - C_{45}^{2}}\sum_{k=1}^{\infty}(\pm 1)^{k-1}kc_k(t). \tag{50}$$

Once the expansion coefficients $c_k(t)$ have been determined numerically by using the time-stepping scheme (25) the elastodynamic stress intensity factor can be calculated by using Eq. (50).

For convenience, a normalized elastodynamic stress intensity factor $\bar{K}_{III}^{\pm}$ is introduced as

$$\bar{K}_{III}^{\pm}(t) = K_{III}^{\pm}(t)/K_{III}^{\mathrm{st}}, \tag{51}$$

where K_{III}^{st} is the static stress intensity factor of an antiplane crack of length $2a$ contained in an infinite anisotropic solid subjected to a remote static stress loading $\sigma_{32}^{\mathrm{st}}$ at infinity, i.e.,

$$K_{III}^{\mathrm{st}} = \sigma_{32}^{\mathrm{st}}\sqrt{\pi a}. \tag{52}$$

6. Scattered displacement and stress fields

While the elastodynamic stress intensity factor is of primary interest to linear elastic fracture mechanics, the scattered displacement and stress fields are of particular interest to ultrasonic quantitative non-destructive evaluation for detecting and characterizing the location, orientation, shape and size of pre-existing cracks, since they are directly related to the scattered displacement and stress fields. The scattered displacement field can be computed by using the representation integral (8), which can be approximated by the following convolution quadrature formula

$$u_3^{\mathrm{sc}}(\mathbf{x}, n\Delta t) = \sum_{j=0}^{n}\mathbf{w}_{(u)}^{n-j}(\mathbf{x}, \Delta t)\mathbf{c}(j\Delta t), \tag{53}$$

where the integration weights $\mathbf{w}_{(u)}^{n}$ are governed by

$$\mathbf{w}_{(u)}^{n}(\mathbf{x}, \Delta t) = w_{(u)k}^{n}(\mathbf{x}, \Delta t) = \frac{r^{-n}}{M}\sum_{m=0}^{M-1}\mathbf{W}_{(u)}(\mathbf{x}, p_m)\mathrm{e}^{-2\pi i \cdot nm/M}, \tag{54}$$

with p_m given by Eq. (23), $M = N$, $r^N = \sqrt{\epsilon}$ and

$$\mathbf{W}_{(u)}(\mathbf{x}, p_m) = W_{(u)k}(\mathbf{x}, p_m) = \int_{-a}^{+a}\hat{\sigma}_{323}^{\mathrm{G}}(\mathbf{x}, \mathbf{y}; p_m)\sqrt{a^2 - y_1^2}U_{k-1}(y_1/a)\,\mathrm{d}y_1. \tag{55}$$

Substitution of Eq. (38) into Eq. (55) and use of Eq. (41) result in

$$W_{(u)k}(\mathbf{x}, p_m) = \frac{ka}{4}\exp\big[i(3k+1)\pi/2\big]\mathrm{sgn}(x_2)\int_{-\infty}^{+\infty}\frac{J_k(\xi a)}{\xi}\exp\big[i\xi x_1 - \gamma_{\pm}|x_2|\big]\,\mathrm{d}\xi. \tag{56}$$

The scattered stress field can be obtained by substituting Eq. (53) into Hooke's law (2) as

$$\sigma^{\mathrm{sc}}_{3\alpha}(\mathbf{x}, n\Delta t) = \sum_{j=0}^{n}\mathbf{w}^{n-j}_{(\sigma)\alpha}(\mathbf{x}, \Delta t)\mathbf{c}(j\Delta t), \tag{57}$$

where

$$\left\{\begin{array}{c}\mathbf{w}^n_{(\sigma)1}\\ \mathbf{w}^n_{(\sigma)2}\end{array}\right\} = \left[\begin{array}{cc}C_{55} & C_{45}\\ C_{45} & C_{44}\end{array}\right]\left\{\begin{array}{c}\dfrac{\partial \mathbf{w}^n_{(u)}}{\partial x_1}\\ \dfrac{\partial \mathbf{w}^n_{(u)}}{\partial x_2}\end{array}\right\}. \tag{58}$$

The integration weights given by Eqs. (54) and (58) can be calculated numerically by using FFT.

7. Numerical results and discussions

Let us consider an incident plane SH-wave (horizontally polarized shear wave) of the general form

$$u^{\mathrm{in}}_3(\mathbf{x}, t) = U_3\big[c_{\mathrm{T}}t - q_1(x_1 + a) - q_2x_2\big]\cdot H\big[c_{\mathrm{T}}t - q_1(x_1 + a) - q_2x_2\big], \tag{59}$$

where U_3 is an amplitude factor, q_α is the wave propagation vector defined by

$$q_1 = \sin\theta; \qquad q_2 = \cos\theta \tag{60}$$

with the incidence angle θ, $H[\cdot]$ is the Heaviside function, and c_{T} is the phase velocity of the SH-wave which is governed by

$$c^2_{\mathrm{T}} = (C_{55}q_1 + 2C_{45}q_1q_2 + C_{44}q_2)/\rho. \tag{61}$$

The corresponding incident stress field can be expressed as

$$\sigma^{\mathrm{in}}_{3\alpha}(\mathbf{x}, t) = \sigma^{\mathrm{st}}_{3\alpha}\cdot H\big[c_{\mathrm{T}}t - q_1(x_1 + a) - q_2x_2\big], \tag{62}$$

in which the static stress components $\sigma^{\mathrm{st}}_{3\alpha}$ are given by

$$\sigma^{\mathrm{st}}_{3\alpha}(\mathbf{x}, t) = \left\{\begin{array}{c}\sigma^{\mathrm{st}}_{31}\\ \sigma^{\mathrm{st}}_{32}\end{array}\right\} = U_3\left[\begin{array}{cc}C_{55} & C_{45}\\ C_{45} & C_{44}\end{array}\right]\left\{\begin{array}{c}q_1\\ q_2\end{array}\right\}. \tag{63}$$

The traction vector $\mathbf{f}^n$ arising in the time-stepping scheme (25) can be integrated analytically by substituting Eq. (62) into Eq. (22). One obtains for a normal incidence ($\theta = 0^\circ$)

$$f^{\,n}_{\,l} = (-1)^{l+1}\sigma^{\mathrm{st}}_{32}\left\{\begin{array}{ll}\dfrac{\pi a^2}{2}, & l = 1,\\ 0, & l\neq 1,\end{array}\right. \tag{64}$$

while for an oblique incidence ($\theta\neq 0^\circ$)

$$f_l^n = (-1)^{l+1}\sigma_{32}^{\mathrm{st}}\begin{cases}\left[\dfrac{1}{2}\theta - \dfrac{1}{4}\sin(2\theta)\right]_{\theta^*}^{\pi}, & l=1,\\ \left[\dfrac{1}{2(l-1)}\sin(l-1)\theta - \dfrac{1}{2(l+1)}\sin(l+1)\theta\right]_{\theta^*}^{\pi}, & l\neq 1,\end{cases} \tag{65}$$

where

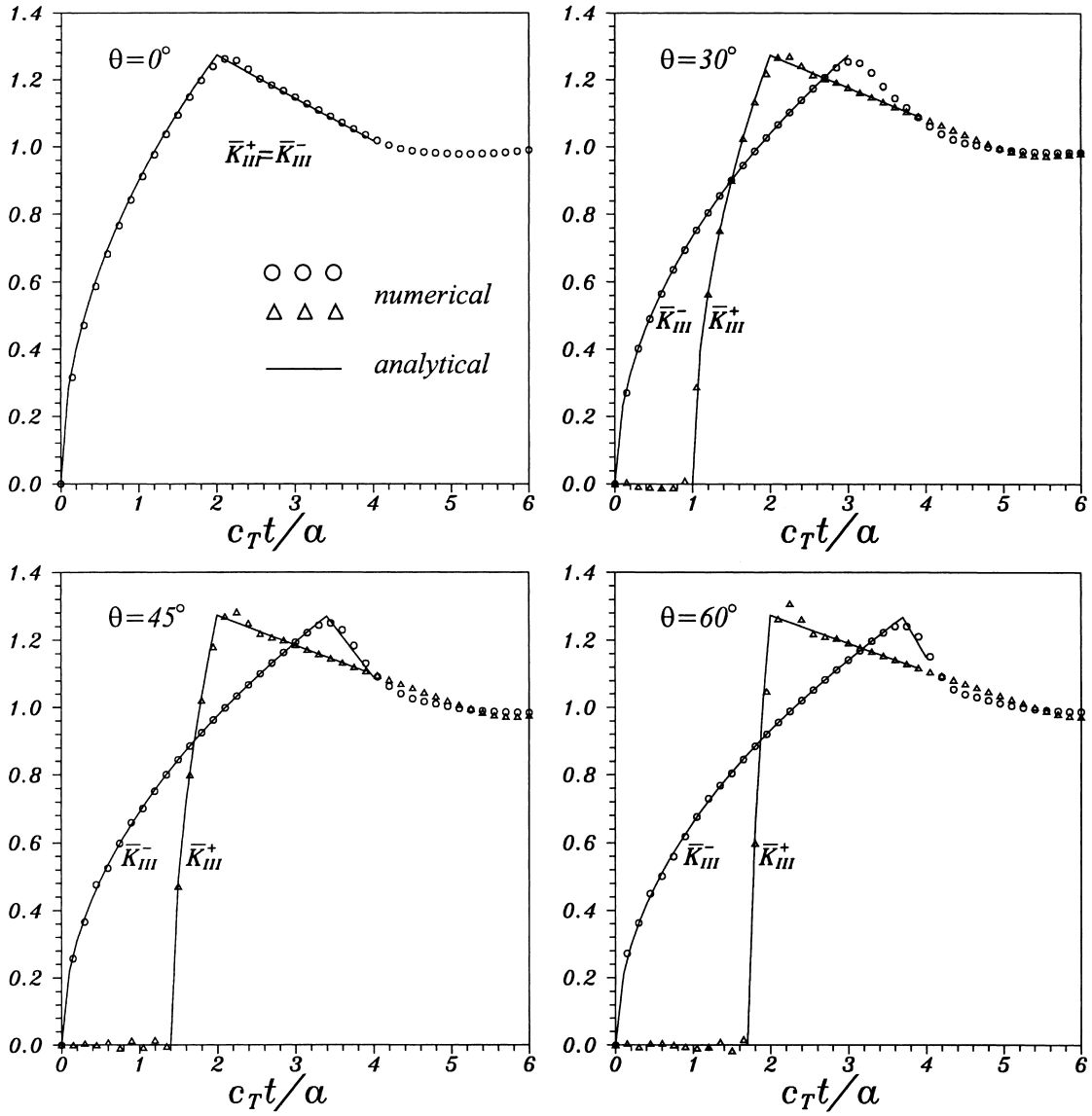

Fig. 3. Normalized dynamic stress intensity factors (isotropic solids).

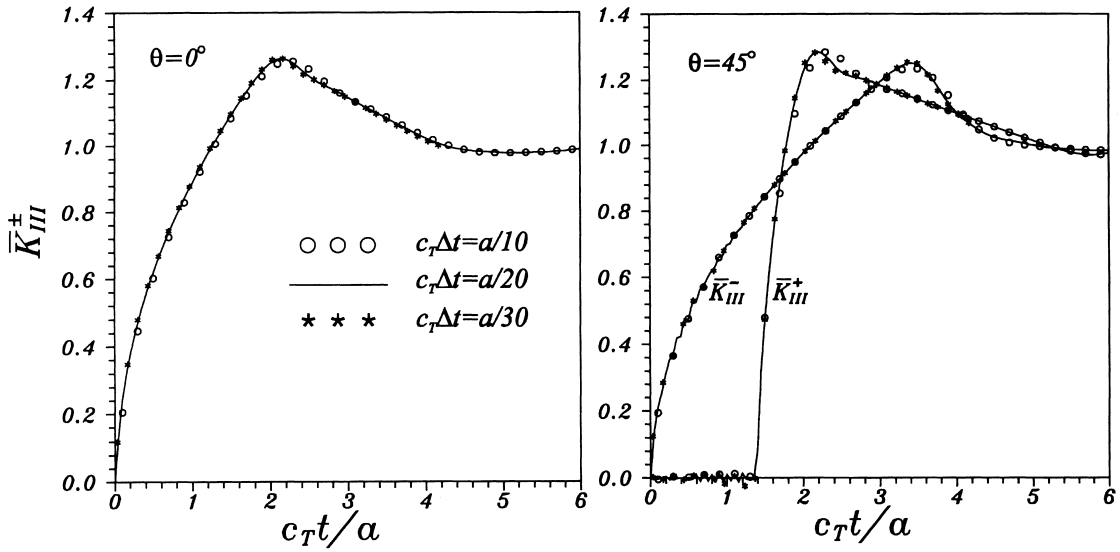

Fig. 4. Influence of time-step $c_T\Delta t$ on $\bar{K}^{\pm}_{III}$-factors (isotropic solids, $\theta = 0^\circ$ and 45°).

$$\theta^* = \arccos\left[\min\left(1, \frac{c_T(n\Delta t)}{\sin\theta} - 1\right)\right]. \tag{66}$$

To solve Eq. (25) numerically, the upper limits $K = L$ of k and l arising in A^n_{kl} have to be truncated. In general, the truncation needed depends on the wave incidence angle θ and the material anisotropy. By trial and error it is concluded that to keep the error of the numerical results less than 3% it is generally

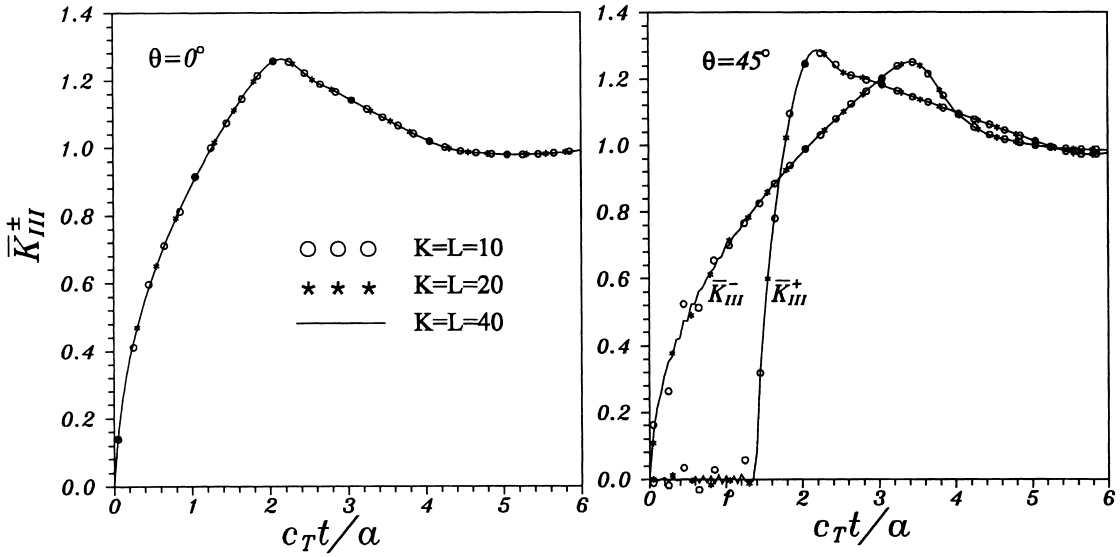

Fig. 5. Influence of $K = L$ on $\bar{K}^{\pm}_{III}$-factors (isotropic solids, $\theta = 0^\circ$ and 45°).

sufficient to take $K = L = 10$. A discussion on the influences of the time-step Δt and the truncation limits $K = L$ on the numerical results is given below. The infinite integral of Eq. (46) is evaluated numerically by using an adaptive Romberg quadrature method in conjunction with the truncation method. The upper limit of the integration is taken as $\xi a = 30$. The parameters used in the computation of the system matrix $\mathbf{A}^n$ defined by Eq. (21) are: $M = N$, $\epsilon = 10^{-10}$ and $r^N = \sqrt{\epsilon}$.

To test the accuracy of the present numerical method, an isotropic solid containing a crack of length $2a$ is first considered. This problem was solved analytically by Thau and Lu (1970) by Wiener–Hopf method. For four different values of the wave incidence angle θ, the normalized elastodynamic stress intensity factors are shown in Fig. 3, versus the dimensionless time $c_T t/a$. Here, $c_T = \sqrt{\mu/\rho}$ where μ is the shear modulus and ρ is the mass density of the solid. Numerical calculations were carried out with $K = L = 40$ and $c_T \Delta t = a/20$. A comparison of the present numerical results with the analytical results of Thau and Lu (1970) shows very good agreements in all cases, which confirms the high accuracy of the present numerical method.

The dependence of the numerical solution on the choice of the time-step $c_T \Delta t$ is shown in Fig. 4. Here, $K = L = 40$ was used. It is shown in Fig. 4 that a smaller time-step than $c_T \Delta t = a/20$ does not influence the numerical results significantly and the time-step $c_T \Delta t = a/20$ is sufficient. Thus, all results presented below are obtained with a time-step $c_T \Delta t = a/20$. Fig. 4 confirms also the conclusions of Gaul and Schanz (1999), Schanz and Antes (1997a, 1997b) and Schanz (1998, 1999) that the time-domain BIE method based on the convolution quadrature of Lubich (1988a, 1988b) is less sensitive to the choice of the time-step, though the collocation method for the spatial discretization of the BIEs has been applied by these authors. For all three values of the time-step $c_T \Delta t = a/10$, $a/20$ and $a/30$ used here, the present method provides stable results, at least in the time range considered.

Fig. 5 shows the dependence of the numerical results on the truncation limits, i.e. the number of Chebyshev polynomials $K = L$ used in the method. Here, the time-step is selected as $c_T \Delta t = a/20$. It is seen on this figure that it is sufficient to take $K = L = 10$ for normally incident waves ($\theta = 0^\circ$), while

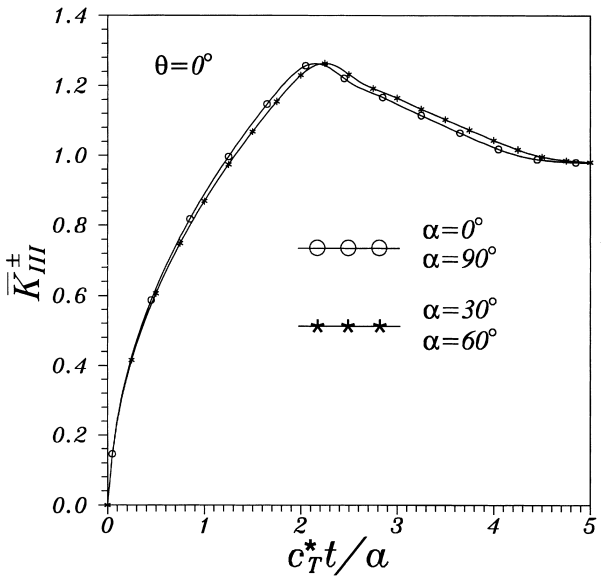

Fig. 6. Normalized dynamic stress intensity factors (anisotropic solids, $\theta = 0^\circ$).

more terms are needed for obliquely incident waves ($\theta \neq 0^\circ$) when the crack-faces are partially loaded. This is the case for instance before the wave-front arrives at the right crack-tip.

Next, we consider a transversely isotropic solid with $C'_{44} = 3.5$ GPa and $C'_{55} = 7.07$ GPa, corresponding to a Graphite–Epoxy composite. If the crack-plane, i.e. x_1-axis does not coincide with one of the principal axes of the material symmetry, i.e. x'_1- or x'_2-axis, a general anisotropy occurs (see Fig. 2). The elastic constants C_{44}, C_{45} and C_{55} in the x_1–x_2-system are related to the elastic constants C'_{44} and C'_{55} in the x'_1–x'_2-system by

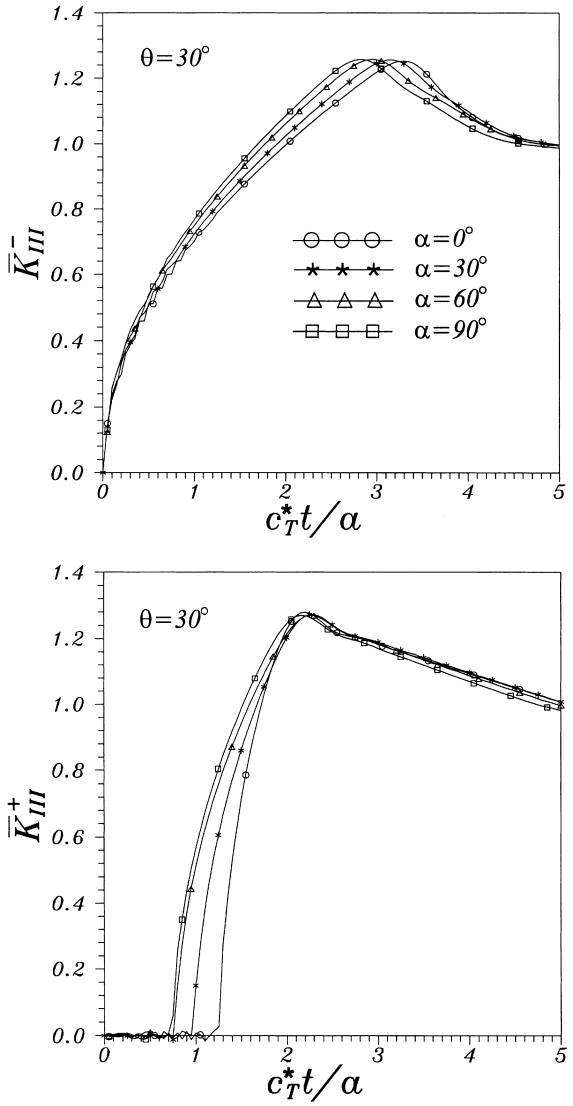

Fig. 7. Normalized dynamic stress intensity factors (anisotropic solids, $\theta = 30^\circ$).

$$\begin{bmatrix} C_{55} & C_{45} \\ C_{45} & C_{44} \end{bmatrix} = \begin{bmatrix} C'_{55}\cos^2\alpha + C'_{44}\sin^2\alpha & \frac{1}{2}\sin(2\alpha)\left(C'_{55} - C'_{44}\right) \\ \text{symmetric} & C'_{55}\sin^2\alpha + C'_{44}\cos^2\alpha \end{bmatrix} \tag{67}$$

where α is the inclination angle of the crack-plane, i.e. x_1-axis, with respect to the x_1'-axis (see Fig. 2). In the special cases $\alpha = 0^\circ$ and $\alpha = 90^\circ$, the crack-plane coincides with one of the axes of material symmetry and the transverse isotropy is recovered. Numerical calculations were carried out with $K = L = 40$ and $c_T^*\Delta t = a/20$, where $c_T^* = \sqrt{C_{55}/\rho}$.

For several values of the inclination angle α corresponding to different degree of material anisotropy,

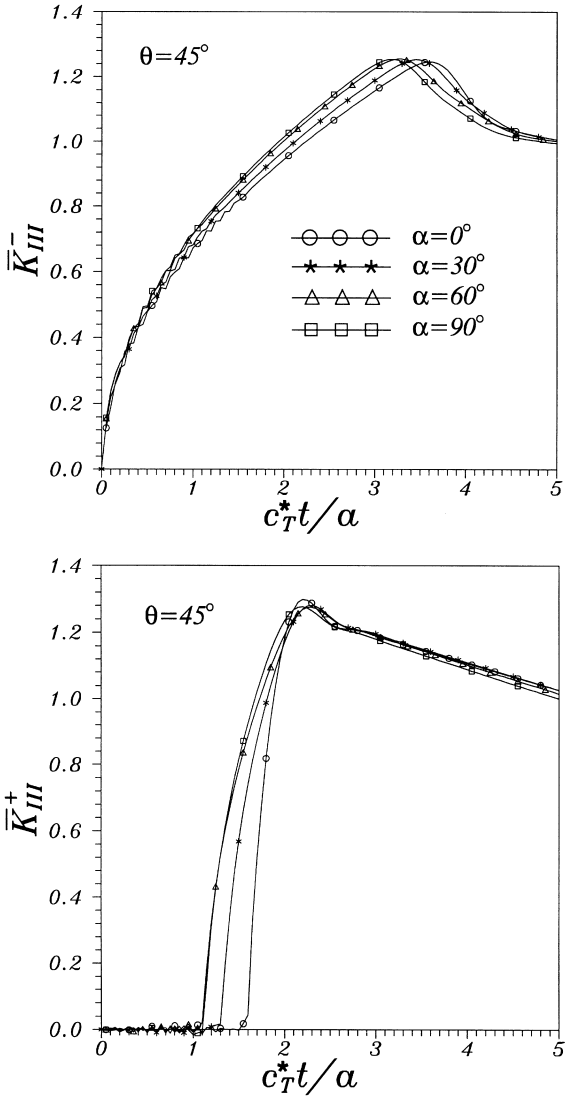

Fig. 8. Normalized dynamic stress intensity factors (anisotropic solids, $\theta = 45^\circ$).

the normalized elastodynamic stress intensity factors are shown in Figs. 6–9, versus the dimensionless time $c_T^* t/a$. The global behavior of the normalized dynamic stress intensity factor is similar to that for isotropic case. Once the wave-front arrives at the crack-tips, the dynamic stress intensity factors increase very rapidly with increasing time, after reaching a maximum they then decrease with increasing time. In the long-time limit $t \to \infty$, the dynamic stress intensity factors approach their corresponding static limits K_{III}^{st}, i.e., $\bar{K}_{III}^{\pm} = 1$. It is interesting to mention that the normalized dynamic stress intensity factors due to normally incident waves ($\theta = 0^\circ$) are identical for $\alpha = 0^\circ$ and 90° corresponding to transversely isotropic cases, and they are identical to that for isotropic case as given in Fig. 3. For $\alpha = 30^\circ$ and 60° corresponding to a general anisotropy, the normalized dynamic stress intensity factors due to normally

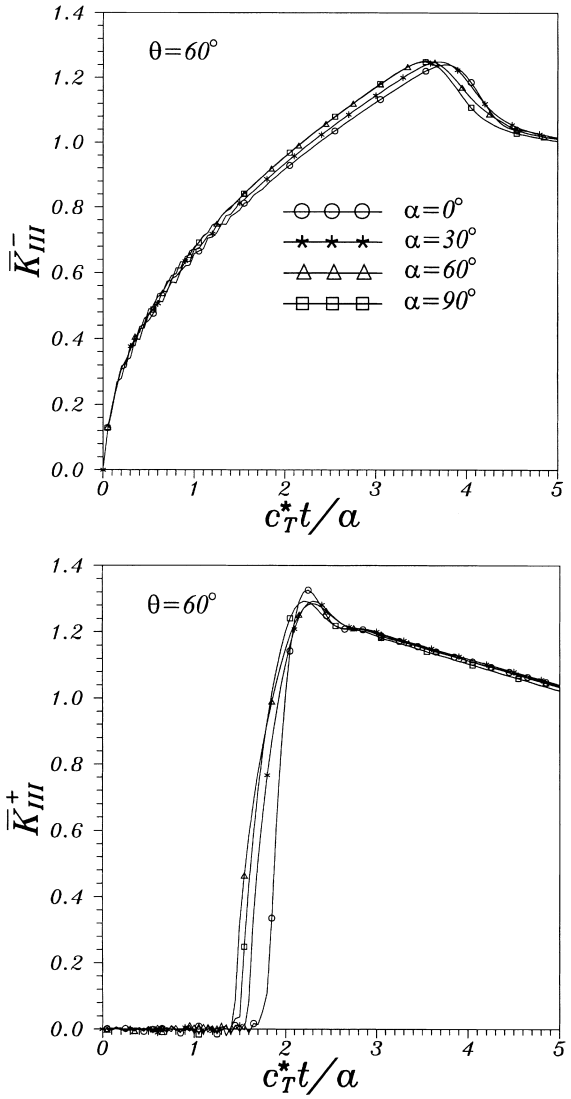

Fig. 9. Normalized dynamic stress intensity factors (anisotropic solids, $\theta = 60^\circ$).

incident waves ($\theta = 0^\circ$) are again identical and they distinguish only slightly from those for the isotropic case or the transversely isotropic case, i.e., $\alpha = 0^\circ$ or 90°. For obliquely incident waves, i.e.,$\theta \neq 0^\circ$, the material anisotropy shifts the maximum normalized dynamic stress intensity factors to an eventually larger or smaller value of the normalized time $c_T^* t/a$, but it does not influence the global behavior of the normalized dynamic stress intensity factors. In the long-time limit $t \to \infty$, the material anisotropy does not alter the normalized dynamic stress intensity factors as it should be. The peak values of the normalized dynamic stress intensity factors depend only weekly on the material anisotropy. This implies that the dynamic overshoot of the dynamic stress intensity factors in anisotropic solids is comparable in amplitude to that for isotropic solids, at least for antiplane cracks considered here.

8. Conclusions

Transient elastodynamic analysis of an antiplane crack in anisotropic solids is performed by using a time-domain traction BIE method. The temporal convolution arising in the time-domain BIE is approximated by a convolution quadrature method developed by Lubich (1988a, 1988b), while the spatial variation of the crack-opening-displacement is approximated by a series of Chebyshev polynomials. By adopting a Galerkin method, a system of linear algebraic equations is obtained from the time-domain BIE. A time-stepping scheme is presented for solving the linear algebraic equations. Numerical examples for isotropic solids show that the present method is highly accurate and stable. The influence of the material anisotropy on the dynamic stress intensity factors is investigated numerically by using several examples.

The present time-domain BIE method uses Laplace-domain in lieu of time-domain Green's functions which are frequently applied in usual time-domain BIE formulations. The method can be extended to two-dimensional inplane crack problems which will be reported in a future paper. The method is especially suited for unbounded domains with straight cracks. For curved cracks or straight cracks in bounded domains, the method can be modified by using other more suitable Laplace-domain Green's functions for anisotropic solids, which can be extracted from the available fundamental solutions of Wang and Achenbach (1994). In this case, it might be advantageous using the collocation method for spatial discretizations of the BIEs, since the Galerkin method involves double or triple integrals which can in general not be integrated analytically. This implies that the Galerkin method for such cases requires much more computing time for evaluating the system matrix than the collocation method does. Applications of the convolution quadrature of Lubich (1988a, 1988b) for temporal convolution and collocation method for spatial discretizations of the time-domain BIEs have been presented by Schanz and Antes (1997a, 1997b), Shanz (1998, 1999), and Gaul and Schanz (1999) for viscoelastic and elastodynamic initial-boundary value problems. One important advantage of the method over the conventional time-domain BIE method is that the method is more stable and less sensitive to the choice of the applied time-steps. Another advantage of the method is that it can also be applied for cases where the Laplace-domain but not the time-domain Green's functions are available in closed or simple forms.

Acknowledgements

Many thanks to Professor Dr. C. Lubich, Institute of Mathematics, University of Tübingen, Germany, and Dr. -Ing. M. Schanz, Institute of Applied Mechanics, TU Braunschweig, Germany, for providing the author their published works and fruitful discussions on the convolution quadrature method.

Appendix A. Convolution quadrature

In this appendix, the convolution quadrature developed by Lubich (1988a, 1988b) is summarized. Details on the method can be found in the published works of Lubich (1988a, 1988b, 1994) and Lubich and Schneider (1992).

They key idea of the convolution quadrature is the approximation of the Riemann convolution

$$f(t) = g(t) * h(t) = \int_0^t g(t-\tau)h(\tau)\,\mathrm{d}\tau \tag{68}$$

by

$$f(n\Delta t) = \sum_{j=0}^{n} \omega_{n-j}(\Delta t)h(j\Delta t), \quad n = 0, 1, \ldots, N, \tag{69}$$

where the time t is divided into N equal time-steps Δt, i.e $t = n\Delta t$, and ω_{n-j} is the integration weights. To derive this quadrature formula, we rewrite Eq. (68) as

$$f(t) = \int_0^t \left[\frac{1}{2\pi i} \int_{C-i\infty}^{C+i\infty} \hat{g}(p)\mathrm{e}^{\,p(t-\tau)}\,\mathrm{d}p \right] h(\tau)\,\mathrm{d}\tau = \frac{1}{2\pi i} \int_{C-i\infty}^{C+i\infty} \hat{g}(p) \int_0^t \mathrm{e}^{\,p(t-\tau)} h(\tau)\,\mathrm{d}\tau\,\mathrm{d}p, \tag{70}$$

where use is made of the inverse Laplace transform

$$g(t-\tau) = \frac{1}{2\pi i} \int_{C-i\infty}^{C+i\infty} \hat{g}(p)\mathrm{e}^{\,p(t-\tau)}\,\mathrm{d}p \tag{71}$$

with the Laplace transform $\hat{g}(p)$ of the function $g(t)$. Introducing the function

$$y(t) = \int_0^t \mathrm{e}^{\,p(t-\tau)} h(\tau)\,\mathrm{d}\tau \tag{72}$$

for the inner integral of Eq. (70) one obtains from Eq. (70)

$$f(t) = \frac{1}{2\pi i} \int_{C-i\infty}^{C+i\infty} \hat{g}(p) y(t)\,\mathrm{d}p. \tag{73}$$

The function $y(t)$ satisfies the following differential equation of first order with the initial condition $y(0)$ at $t = 0$

$$\dot{y}(t) = py(t) + h(t); \quad y(0) = 0. \tag{74}$$

The differential equation (74) can be approximated by a linear multistep method which results in

$$\sum_{j=0}^{k} \alpha_j y_{n-j} = \Delta t \sum_{j=0}^{k} \beta_j \left[p y_{n-j} + h_{n-j} \right], \quad n \geq 0 \tag{75}$$

with $y_{n-j} = y((n-j)\Delta t$, $h_{n-j} = h((n-j)\Delta t$, and the starting values $y_{-k} = \cdots = y_{-1} = 0$. Multiplying both sides of Eq. (75) with ζ^n ($|\zeta| \leq 1$), using the formal power series representation

$$y(t) = y(\zeta) = \sum_{n=0}^{\infty} y_n \zeta^n; \qquad h(t) = h(\zeta) = \sum_{n=0}^{\infty} h_n \zeta^n \tag{76}$$

and summing up over n from 0 to ∞ one obtains

$$y(t) = y(\zeta) = \left[\frac{\delta(\zeta)}{\Delta t} - p \right]^{-1} h(\zeta), \tag{77}$$

with the quotient of the generating polynomials of the multistep method $\delta(\zeta)$

$$\delta(\zeta) = \frac{\sum_{j=0}^{k} \alpha_j \zeta^{\,j}}{\sum_{j=0}^{k} \beta_j \zeta^{\,j}}. \tag{78}$$

Of particular interest to the present analysis is the multistep method which is A-stable and of order 2, i.e.

$$\mathrm{Re}\big[\delta(\zeta)\big] \geq 0, \quad \text{for } |\zeta| \leq 1, \tag{79}$$

$$\frac{1}{\Delta t}\delta(\mathrm{e}^{-\Delta t}) = 1 + O(\Delta t^2), \quad \text{for } \Delta t \to 0. \tag{80}$$

Well-known examples of second-order A-stable methods are the backward difference formula with $\delta(\zeta) = \sum_{j=1}^{2} (1-\zeta)^{\,j}/j$ and the trapezoidal rule with $\delta(\zeta) = 2(1-\zeta)/(1+\zeta)$.

Substituting Eqs. (76) and (77) into Eq. (73) and using Cauchy's integral formula for evaluating the integral (73) one obtains

$$f(t) = \sum_{n=0}^{\infty} f(n\Delta t)\zeta^n = \hat{g}\left(\frac{\delta(\zeta)}{\Delta t}\right) \sum_{n=0}^{\infty} h(n\Delta t)\zeta^n, \tag{81}$$

where the following asymptotic behavior of $\hat{g}(p)$ is assumed

$$|\hat{g}(p)| \to 0 \quad \text{for } \mathrm{Re}(p) \geq 0,\ |p| \to \infty. \tag{82}$$

Substituting the formal power series expression for $\hat{g}(\zeta)$

$$\hat{g}\left(\frac{\delta(\zeta)}{\Delta t}\right) = \sum_{n=0}^{\infty} \omega_n(\Delta t)\zeta^n \tag{83}$$

into Eq. (81) and using Cauchy's product formula for two series, Eq. (81) can be rewritten as

$$\sum_{n=0}^{\infty} f(n\Delta t)\zeta^n = \sum_{n=0}^{\infty} \sum_{j}^{n} \omega_{n-j}(\Delta t) h(j\Delta t)\zeta^n. \tag{84}$$

Taking the nth coefficient of the power series (84) results in finally the convolution quadrature (69). The integration weights $\omega_n(\Delta t)$ arising in Eq. (83) is defined by

$$\omega_n(\Delta t) = \frac{1}{2\pi}\int_{|\zeta|=r} \hat{g}\left(\frac{\delta(\zeta)}{\Delta t}\right)\zeta^{-n-1}\,\mathrm{d}\zeta, \tag{85}$$

where r is the radius of a circle in the domain of analyticity of $\hat{g}(\zeta)$. This integral can be approximated with high accuracy by a trapezoidal rule with M equal steps $2\pi/M$ (Lubich, 1988b) as

$$\omega_n(\Delta t) = \frac{r^{-n}}{M}\sum_{m=0}^{M-1}\hat{g}\left(\frac{\delta(\zeta_m)}{\Delta t}\right)\mathrm{e}^{-2\pi i\cdot nm/M}, \tag{86}$$

in which $\delta(\zeta_m)$ and ζ_m are defined by Eq. (23).

References

Abramowitz, M., Stegun, I.A., 1972. Handbook of Mathematical Functions. Dover, New York.

Albuquerque, E.L., Sollero, P., Aliabadi, M.H., 1999. The dual boundary element method applied to dynamic fracture mechanics in anisotropic solids. In: Int. Conf. on Boundary Element Techniques, 6–8 July, London, UK.

Ang, W.T., 1987. Transient response of a crack in an anisotropic strip. Acta Mechanicca 70, 97–109.

Ang, W.T., 1988. A crack in an anisotropic layered material under the action of impact loading. ASME J. Appl. Mech 55, 120–125.

Ang, W.T., Clements, D.L., Dehghan, M., 1993. Scattering and diffraction of SH-waves by multiple planar cracks in an anisotropic half-space: a hypersingular integral formulation. Int. J. Solids Struct 30, 1301–1312.

Danyluk, H.T., Singh, B.M., 1984. Closed form solutions for a finite length crack moving in an orthotropic layer of finite thickness. Letters Appl. Engrg. Sci 22, 637–644.

Das, S., Patra, B., 1998. Stress intensity factors for moving interfacial crack between bonded dissimilar fixed orthotropic layers. Computers & Structures 69, 459–472.

Dhawan, G.K., 1982. Interaction of elastic waves by a Griffith crack in an infinite transversely-isotropic medium. Int. J. Fract 19, 29–37.

Dhawan, G.K., 1983. Interaction of SV-waves by a Griffith crack in an infinite transversely-isotropic medium. Int. J. Fract 20, 103–110.

Dominguez, J., Sáez, A., 1992. Boundary element analysis of 3-D dynamic crack problems in isotropic and transversely isotropic solids. In: Fourth Word Congress on Computational Mechanics, June 29–2 July, Buenos Aires, Argentina.

Gaul, L., Schanz, M., 1999. A comparative study of three boundary element approaches to calculate the transient response of viscoelastic solids with unbounded domains. Comput. Meth. in Appl. Mech. Eng. 179, 111–123.

Itou, S., 1996. Dynamic stress intensity factors of two collinear cracks in orthotropic medium subjected to time-harmonic disturbance. Theor. and Appl. Fract. Mech 25, 155–166.

Itou, S., Haliding, H., 1997. Dynamic stress intensity factors around two parallel cracks in an infinite-orthotropic plane subjected to incident harmonic stress waves. Int. J. Solids Structures 34, 1145–1165.

Karim, M.R., Kundu, T., 1988. Transient surface response of layered isotropic and anisotropic half-spaces with interface cracks: SH case. Int. J. Fract 37, 245–262.

Karim, M.R., Kundu, T., 1991. Dynamic response of an orthotropic half-space with a subsurface crack: in-plane case. ASME J. Appl. Mech 58, 988–995.

Kassir, M.K., Bandyopadhyay, K.K., 1983. Impact response of a cracked orthotropic medium. ASME J. Appl. Mech 50, 630–636.

Kassir, M.K., Tse, S., 1983. Moving Griffith crack in an orthotropic material. Int. J. Engrg. Sci 21, 315–325.

Kundu, T., 1990. Scattering of torsional waves by a circular crack in a transversely isotropic solid. J. Acoust. Soc. Amer 88, 1975–1980.

Kundu, T., Boström, A., 1991. Axisymmetric scattering of a plane longitudinal wave by a circular crack in a transversely isotropic solid. ASME J. Appl. Mech 58, 695–702.

Kundu, T., Boström, A., 1992. Elastic wave scattering by a circular crack in a transversely isotropic solid. Wave Motion 15, 285–300.

Kuo, A.-Y., 1984a. Transient stress intensity factors of an interfacial crack between two dissimilar anisotropic half-spaces. Part 1: Orthotropic materials. ASME J. Appl. Mech 51, 71–76.

Kuo, A.-Y., 1984b. Transient stress intensity factors of an interfacial crack between two dissimilar anisotropic half-spaces. Part 2: Fully anisotropic materials. ASME J. Appl. Mech 51, 780–786.

Liu, G.R., Achenbach, J.D., 1995. Strip element method to analyze wave scattering by cracks in anisotropic laminated plates. ASME J. Appl. Mech 62, 607–613.

Lobanov, E.V., Novichkov, Y.N., 1981. Diffraction of SH-waves by an oblique crack in an orthotropic half-space. Soviet Appl. Mech 17, 610–615.

Lubich, C., 1988a. Convolution quadrature and discretized operational calculus. Part I. Numer. Math 52, 129–145.

Lubich, C., 1988b. Convolution quadrature and discretized operational calculus. Part II. Numer. Math 52, 413–425.

Lubich, C., Schneider, R., 1992. Time discretization of parabolic boundary integral equations. Numer. Math 63, 455–481.

Lubich, C., 1994. On the multistep time discretization of linear initial-boundary value problems and their boundary integral equations. Numer. Math 67, 365–389.

Mattsson, J., 1996. Modeling of scattering by cracks in anisotropic solids — application to ultrasonic detection. Ph.D. Thesis, Div. Mech., Chalmers University of Technology, Göteborg, Sweden.

Mattsson, J., Niklasson, A.J., 1997. Ultrasonic 2-D SH crack detection in anisotropic solids. J. Nondestr. Eval 16, 31–41.

Mattsson, J., Niklasson, A.J., Eriksson, A., 1997. Three-dimensional ultrasonic crack detection in anisotropic materials. Res. Nondestr. Eval 9, 59–79.

Niklasson, A.J., 1997. Elastic wave propagation in anisotropic media — application to ultrasonic NDT. Ph.D. Thesis, Div. Mech., Chalmers University of Technology, Göteborg, Sweden.

Norris, A.N., Achenbach, J.D., 1984. Elastic wave diffraction by a semi-infinite crack in a transversely isotropic material. Quart. J. Mech. Appl. Math 37, 565–580.

Ohyoshi, T., 1973a. Effect of orthotropy on singular stresses produced near a crack tip by incident SH-waves. ZAMM Z. Angew. Math. Mech 53, 409–411.

Ohyoshi, T., 1973b. Effect of orthotropy on singular stresses for a finite crack. ASME J. Appl. Mech 40, 491–497.

Padovan, J., 1998. Modelling crack propagation in anisotropic media. Eng. Fract. Mech 60, 457–478.

Piva, A., 1986. Elastodynamic crack problems in an anisotropic medium through a complex variable approach. Quart. Appl. Math 44, 441–445.

Piva, A., 1987. An alternative approach to elastodynamic crack problems in an orthotropic medium. Quart. Appl. Math 45, 97–104.

Piva, A., Hasan, W., 1996. Effect of orthotropy on the intersonic shear crack propagation. ASME J. Appl. Mech 63, 933–938.

Pramanik, R.K., Pal, S.C., Ghosh, M.L., 1998. Transient response due to a pair of antiplane point impact loading on the faces of a finite Griffith crack at the bimaterial interface of anisotropic solids. Int. J. Eng. Sci 36, 1197–1213.

Rizza, R., Nair, S., 1998. A penny-shaped crack in a transversely isotropic material under non-axisymmetrical impact loads. Int. J. Solids Structures 36, 35–64.

Rubio-Gonzalez, C., Mason, J.J., 1999. Response of finite cracks in orthotropic materials due to concentrated impact shear loads. ASME J. Appl. Mech 66, 485–491.

Sáez, A., Domínguez, J., 1999. Scattering of elastic waves by cracks in 3-D transversely isotropic solids. In: Int. Conf. on Boundary Element Techniques, 6–8 July 1999, London, UK.

Sarkar, J., Mandal, S.C., Ghosh, M.L., 1995. Diffraction of elastic waves by three coplanar Griffith cracks in an orthotropic medium. Int. J. Eng. Sci 33, 163–177.

Schanz, M., Antes, H., 1997a. A new visco- and elastodynamic time domain boundary element formulation. Computational Mechanics 20, 452–459.

Schanz, M., Antes, H., 1997b. Application of operational quadrature methods in time domain boundary element methods. Meccanica 32, 179–186.

Schanz, M., 1998. Multistep time discretization of boundary integral equations in dynamics. In: Atluri, S.N., O'Donoghue, P.E. (Eds.), Modelling and Simulation Based Engineering, vol. I. Tech Science Press, Palmdale, USA, pp. 223–228.

Schanz, M., 1999. A time domain boundary integral equation for Euler–Bernoulli beams. ZAMM Zeitschr. Angew. Math. Mech., in press.

Shen, S., Kuang, Z.-B., 1998. Wave scattering from an interface crack in laminated anisotropic media. Mech. Res. Commun 25, 509–517.

Shindo, Y., Nozaki, H., Higaki, H., 1986. Impact response of a finite crack in an orthotropic strip. Acta Mechanicca 62, 87–104.

Shindo, Y., Nozaki, H., 1987. Impact response of a transversely isotropic cylinder with a penny shaped crack. Int. J. Solids Structures 23, 187–199.

Thau, S.A., Lu, T.H., 1970. Diffraction of transient horizontal shear waves by a finite crack and a finite rigid ribbon. Int. J. Engng. Sci 8, 857–874.

Tsai, Y.M., 1973. Exact stress distribution, crack shape and energy of a running penny-shaped crack in an infinite elastic solid. Int. J. Fract 9, 157–169.

Tsai, Y.M., 1982. Penny-shaped crack in a transversely isotropic plate of finite thickness. Int. J. Fract 20, 81–89.

Tsai, Y.M., 1988. Dynamic penny-shaped crack in a transversely isotropic material. Eng. Fract. Mech 31, 977–984.

Tsai, Y.M., 1989. Torsional vibration of a penny-shaped crack in a transversely isotropic material. In: Salama, K., et al. (Eds.), Advances in Fracture Research ICF 7, vol. 3. Pergamon Press, Oxford, pp. 2363–2368.

Wang, C.-Y., Achenbach, J.D., 1994. Elastodynamic fundamental solutions for anisotropic solids. Geophys. J. Int 118, 384–392.

Wang, C.-Y., Achenbach, J.D., Hirose, S., 1996. Two-dimensional time domain BEM for scattering of elastic waves in solids of general anisotropy. Int. J. Solids Structures 33, 3843–3864.

Zhang, Ch., 1992. Elastodynamic analysis of a periodic array of mode III cracks in transversely isotropic solids. ASME J. Appl. Mech 59, 366–371.

Zhang, Ch., Gross, D., 1993. Interaction of antiplane cracks with elastic waves in transversely isotropic materials. Acta Mechanica 101, 231–247.